Lattice Boltzmann method for thermal flow simulation on standard lattices

Nikolaos I. Prasianakis* and Iliya V. Karlin†
Aerothermochemistry and Combustion Systems Laboratory, Institute of Energy Technology, ETH Zurich, 8092 Zurich, Switzerland
(Received 23 March 2007; published 9 July 2007)

The recently introduced consistent lattice Boltzmann model with energy conservation [S. Ansumali and I. V. Karlin, Phys. Rev. Lett. **95**, 260605 (2005)] is extended to the simulation of thermal flows on standard lattices. The two-dimensional thermal model on the standard square lattice with nine velocities is developed and validated in the thermal Couette and Rayleigh-Bénard natural convection problems.

DOI: 10.1103/PhysRevE.76.016702 PACS number(s): 47.11.−j, 05.70.Ln

I. INTRODUCTION

The lattice Boltzmann (LB) method is a powerful approach to hydrodynamics, with applications ranging from large Reynolds number flows to flows at a micron scale, porous media, and multiphase flows [1]. The LB method solves a fully discrete kinetic equation for populations $f_i(x,t)$, designed in a way that it reproduces the target equations of continuum mechanics in the hydrodynamic limit. Populations correspond to discrete velocities c_i, $i=1,\ldots,N$, which fit into a regular spatial lattice with the nodes x. This enables a simple and efficient "stream-along-links-and-equilibrate-at-nodes" realization of the LB algorithm.

In the case of incompressible flows, where the target equations are Navier-Stokes equations at low Mach number, the LB method proves to be competitive to conventional methods of computational fluid dynamics [2]. In that case, the LB models on the so-called standard lattices with a relatively small number of velocities ($N=9$ in two dimensions, see Fig. 1, and $N=15$, 19, and 27 in three) are available and most commonly used. In this paper, we will follow the usual nomenclature and indicate the models as $DMQN$ where $M=2,3$ is the spatial dimension and N the number of the discrete velocities of the model.

However, the situation is quite different with LB models for compressible thermal flows. In spite of a number of recent suggestions, a commonly accepted LB model for thermal flows has not yet been established, to the best of our knowledge. A reason for such a difference between the isothermal and thermal cases is mainly because it is not straightforward to incorporate the temperature into the lattice equilibrium when using the standard lattices, and simultaneously to satisfy a number of conditions for recovering the Navier-Stokes and Fourier equations for compressible flows [3]. At present, two major approaches to constructing thermal LB models can be distinguished. In the first approach, lattices with a larger number of discrete velocities or off-lattice velocity sets are considered to enable local energy conservation and isotropy [4,5]. In the second approach, two copies of the standard lattices are considered, one of which is designed to treat the density and momentum and the other—the energy density. The standard isothermal LB model on the first lattice is considered, and the coupling between the lattices is enhanced by introducing force terms in order to recover viscous heat dissipation [6]. However, both these approaches inevitably deal with more discrete speeds than the standard single-lattice LB models which leads to reducing efficiency.

Recently, a so-called consistent LB model has been introduced in Ref. [7]. It has been shown that it is possible to construct the LB model with energy conservation on the standard lattices in such a way that the spurious bulk viscosity of isothermal LB models is eliminated, and that the Navier-Stokes and Fourier equations are recovered once the temperature is varied in a small neighborhood of a reference temperature. However, the consistent LB model is limited to weakly compressible flows and is not yet sufficient to simulate thermal flows. The reason for that is the low symmetry of the standard lattices which leads to accumulation of deviations of the resulting hydrodynamic equations from their Navier-Stokes and Fourier counterparts. It should be noted, however, that the consistent LB model with energy conservation on standard lattices should be considered as a better and more natural starting point for a development of the thermal LB model as compared to the isothermal model.

In this paper, we complete the program of constructing the thermal LB model on standard lattices as an extension of the consistent LB model [7]. A thermal lattice Boltzmann model is derived on the most commonly used $D2Q9$ lattice as follows: In Sec. II, we revisit the derivation of the local equilibrium of the thermal model, using the method of guided equilibrium [8]. This enables us to enhance Galilean invariance of the consistent LB method for large temperature variations. We shall also identify the remaining deviations in the higher-order moments due to the lattice constraints. In Sec. III, the impact of these deviations on the hydrodynamic equations is identified (algebraic details of the derivation are presented in the Appendix). In Sec. IV, additional terms are introduced in the Boltzmann equation in such a way that all the deviations of the hydrodynamic equations from their Navier-Stokes and Fourier counterparts are eliminated. In addition, further terms are introduced to represent external forces, as well as to tune the Prandtl number of the model. In Sec. V, the discretization in time and space of the kinetic equation of Sec. IV is performed, and a simple numerical algorithm is outlined. In Sec. VI, numerical examples are provided. Simulations of the thermal Couette flow and of the Rayleigh-Bénard natural convection show excellent agreement with theoretical results. The numerical implementation

*prasianakis@lav.mavt.ethz.ch
†Corresponding author. karlin@lav.mavt.ethz.ch

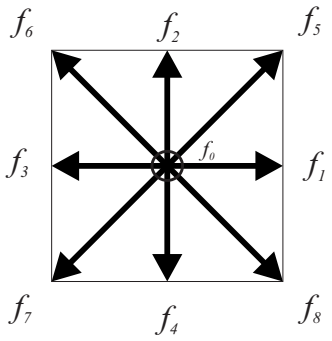

FIG. 1. The $D2Q9$ velocity set.

is summarized in a compact form in Sec. VII. Finally, results are discussed in Sec. VIII.

II. LOCAL EQUILIBRIUM

A. Consistent lattice Boltzmann method

We begin by recalling the construction of the local equilibrium in the consistent lattice Boltzmann method [7,9] on the planar square lattice with nine velocities $c_{i\alpha}$, $i=0,\ldots,8$ (see Fig. 1):

$$c_x = \{0,1,0,-1,0,1,-1,-1,1\},$$
$$c_y = \{0,0,1,0,-1,1,1,-1,-1\}. \tag{1}$$

Equilibrium populations are obtained from minimization of the entropy function H under constraints provided by local conservation laws. For the $D2Q9$ model, the entropy function has the form [10]

$$H = \sum_{i=0}^{8} f_i \ln\left(\frac{f_i}{W_i}\right), \tag{2}$$

where the weights W_i are

$$W = \frac{1}{36}\{16,4,4,4,4,1,1,1,1\}. \tag{3}$$

In the consistent lattice Boltzmann method [7], the local conservations include mass, momentum, and energy,

$$\sum_{i=0}^{8} f_i^{\mathrm{eq}} = \rho,$$
$$\sum_{i=0}^{8} c_{i\alpha} f_i^{\mathrm{eq}} = j_\alpha, \tag{4}$$
$$\sum_{i=0}^{8} c_i^2 f_i^{\mathrm{eq}} = 2\rho T + \frac{j^2}{\rho},$$

where ρ, $j_\alpha=\rho u_\alpha$, and T are the density, momentum, and temperature fields, correspondingly. Note that the consistent lattice Boltzmann construction includes energy conservation among the constraints (4). Note that this is at variance with the standard isothermal lattice Boltzmann method on the same lattice [11] where the entropy function is minimized under the constraints of mass and momentum only [10].

Derivation of the equilibrium populations as a minimizer of the entropy function (2) under constraints (4) can be found in Refs. [7,9], and is not reproduced here. We recall that at the reference temperature $T_0=1/3$, the consistent lattice Boltzmann model recovers the Navier-Stokes-Fourier hydrodynamic equations and results in the nonequilibrium pressure tensor without a spurious bulk viscosity of the standard lattice Boltzmann model. However, the consistent lattice Boltzmann model itself is not yet capable of simulating accurately thermal flows with significant temperature and density variations. In particular, the equilibrium pressure tensor of the consistent lattice Boltzmann model shows deviations of the order of $u^2\Delta T$ (where ΔT is a deviation from the reference temperature) from the target Maxwell-Boltzmann form,

$$P_{\alpha\beta}^{\mathrm{MB}} = \rho T\delta_{\alpha\beta} + \frac{j_\alpha j_\beta}{\rho}. \tag{5}$$

Hence, as the first step towards establishing the lattice Boltzmann method for thermal flow simulations, we need to modify the construction of the equilibrium which would remove this deviation from the pressure tensor.

B. Guided local equilibrium

In order to remove the aforementioned deviation in the equilibrium pressure tensor, we use the method of guided equilibrium introduced in [8] for a generic lattice Boltzmann model. Following [8], we minimize the entropy function (2) under an extended set of conditions which includes the local conservations (4) and the condition which stipulates that the equilibrium pressure tensor $P_{\alpha\beta}^{\mathrm{eq}}$ is in the MB form (5),

$$\sum_{i=0}^{8} c_{i\alpha}c_{i\beta}f_i^{\mathrm{eq}} = \rho T\delta_{\alpha\beta} + \frac{j_\alpha j_\beta}{\rho}. \tag{6}$$

Minimization of the entropy function (2) under the extended list of constraints, Eqs. (4) and (6), leads to the equilibrium populations of the form

$$f_i^{\mathrm{eq}} = w_i \exp\{\mu + \zeta_\alpha c_{i\alpha} + \chi_{\alpha\beta}c_{i\alpha}c_{i\beta} + \gamma c_i^2\}, \tag{7}$$

where summation convention in two repeated spatial indices is assumed, and where μ, ζ_α, $\chi_{\alpha\beta}$, and γ are Lagrange multipliers of the constraints. Their values are found upon substitution of Eq. (7) into Eqs. (4) and (6). Equilibrium at zero velocity ($j_\alpha=0$) can be found exactly and coincides with the one reported in [7,9]. Equilibria at nonzero velocity are then derived by perturbation around the zero-velocity state, and f_i^{eq} are represented in terms of a series in the momentum. For what will follow, expansion up to the fourth order in velocity is required. This solution procedure is quite standard, hence we reproduce only the result in terms of the velocity $u_\alpha = j_\alpha/\rho$:

$$f_0^{\mathrm{eq}} = \rho(T + u_x^2 - 1)(T + u_y^2 - 1),$$
$$f_1^{\mathrm{eq}} = \frac{\rho}{2}(T + u_x + u_x^2)(1 - T - u_y^2),$$

$$f_2^{\mathrm{eq}} = \frac{\rho}{2}(1 - T - u_x^2)(T + u_y + u_y^2),$$

$$f_3^{\mathrm{eq}} = \frac{\rho}{2}(T - u_x + u_x^2)(1 - T - u_y^2),$$

$$f_4^{\mathrm{eq}} = \frac{\rho}{2}(1 - T - u_x^2)(T - u_y + u_y^2),$$

$$f_5^{\mathrm{eq}} = \frac{\rho}{4}(T + u_x + u_x^2)(T + u_y + u_y^2),$$

$$f_6^{\mathrm{eq}} = \frac{\rho}{4}(T - u_x + u_x^2)(T + u_y + u_y^2),$$

$$f_7^{\mathrm{eq}} = \frac{\rho}{4}(T - u_x + u_x^2)(T - u_y + u_y^2),$$

$$f_8^{\mathrm{eq}} = \frac{\rho}{4}(T + u_x + u_x^2)(T - u_y + u_y^2). \tag{8}$$

Note that equilibrium populations at zero velocity remain positive for temperature values $0 < T < 1$. The equilibrium pressure tensor satisfies the MB relation per construction,

$$P_{\alpha\beta}^{\mathrm{eq}} = P_{\alpha\beta}^{\mathrm{MB}}. \tag{9}$$

The properties of the higher-order moments in the equilibrium (8) are studied in the next section.

C. Deviations in higher-order moments

Apart from the equilibrium pressure tensor, also the third- and fourth-order moments of the equilibrium must satisfy the Maxwell-Boltzmann relations in order to recover the Navier-Stokes and the temperature equation in the hydrodynamic limit,

$$\begin{aligned} Q_{\alpha\beta\gamma}^{\mathrm{MB}} &= T(j_\alpha \delta_{\beta\gamma} + j_\beta \delta_{\alpha\gamma} + j_\gamma \delta_{\alpha\beta}) + \frac{j_\alpha j_\beta j_\gamma}{\rho^2}, \\ R_{\alpha\beta}^{\mathrm{MB}} &= T\left(\frac{j^2}{\rho} + 4T\right)\delta_{\alpha\beta} + 6T\frac{j_\alpha j_\beta}{\rho} + \frac{j_\alpha j_\beta j^2}{\rho^3}. \end{aligned} \tag{10}$$

Using the equilibrium populations (8) to evaluate the functions

$$\begin{aligned} Q_{\alpha\beta\gamma}^{\mathrm{eq}} &= \sum_{i=0}^{8} c_{i\alpha} c_{i\beta} c_{i\gamma} f_i^{\mathrm{eq}}, \\ R_{\alpha\beta}^{\mathrm{eq}} &= \sum_{i=0}^{8} c_{i\alpha} c_{i\beta} c_i^2 f_i^{\mathrm{eq}}, \end{aligned} \tag{11}$$

and introducing, for a generic moment M, a deviation M' of its equilibrium value M^{eq} from the Maxwell-Boltzmann value M^{MB},

$$M^{\mathrm{eq}} = M^{\mathrm{MB}} + M', \tag{12}$$

we find the following deviations of the third- and fourth-order moments:

$$\begin{aligned} Q'_{xxx} &= j_x(1 - 3T) - \frac{j_x^3}{\rho^2}, \\ Q'_{yyy} &= j_y(1 - 3T) - \frac{j_y^3}{\rho^2}, \\ R'_{xx} &= (1 - 3T)\rho T + (1 - 6T)\frac{j_x^2}{\rho} - \frac{j_x^4}{\rho^3}, \\ R'_{yy} &= (1 - 3T)\rho T + (1 - 6T)\frac{j_y^2}{\rho} - \frac{j_y^4}{\rho^3}, \\ R'_{xy} &= 2(1 - 3T)\frac{j_x j_y}{\rho} - \frac{j_x j_y j^2}{\rho^3}. \end{aligned} \tag{13}$$

Note that the off-diagonal elements of the third-order moment $Q_{\alpha\beta\gamma}^{\mathrm{eq}}$ already satisfy the Maxwell-Boltzmann relations,

$$Q_{xxy}^{\mathrm{eq}} = Q_{xxy}^{\mathrm{MB}}, \quad Q_{yyx}^{\mathrm{eq}} = Q_{yyx}^{\mathrm{MB}}. \tag{14}$$

Thus the deviation of the contracted third-order moment, $q_\alpha^{\mathrm{eq}} = \Sigma_{i=0}^{8} c_{i\alpha} c_i^2 f_i^{\mathrm{eq}}$ (the energy flux) is due to the deviation of the diagonal elements,

$$q'_\alpha = Q'_{\alpha\alpha\alpha}. \tag{15}$$

Deviations of the diagonal components of the third-order moments are well-known for the low-symmetry $D2Q9$ lattice, and stem from the fact that the velocity set satisfies a relation, $c_{i\alpha}^3 = c_{i\alpha}$. This lattice constraint precludes construction of equilibrium different from Eq. (8) in such a way that also the energy flux would be guided by the Maxwell-Boltzmann relation.

In the next section, we shall identify the impact of the deviations (13) on the hydrodynamic equations. Once this will be done, we shall remove the anomalous terms in the hydrodynamic equations by introducing correction terms into the kinetic equation.

III. DEVIATIONS IN THE HYDRODYNAMIC EQUATIONS

A. Bear BGK model

In this section, the impact of deviations of the moments (13) on the hydrodynamic equations will be identified using the single relaxation time Bhatnagar-Gross-Krook (BGK) model for the collision integral:

$$\partial_t f_i + c_{i\alpha}\partial_\alpha f_i = -\frac{1}{\tau}(f_i - f_i^{\mathrm{eq}}), \tag{16}$$

where τ is the relaxation time, and the equilibrium populations are given by Eq. (8). The hydrodynamic limit of the BGK kinetic equation (16) can be studied via the Chapman-Enskog expansion. Details of the Chapman-Enskog analysis

are given in the Appendix. Here we shall summarize the results of this analysis.

B. Deviations in the momentum equation

To the first order of the Chapman-Enskog expansion, the momentum equation reads

$$\partial_t j_\alpha + \partial_\beta P^{\mathrm{MB}}_{\alpha\beta} + \partial_\beta P^{\mathrm{neq}}_{\alpha\beta} = -\partial_\gamma P''_{\alpha\gamma}, \tag{17}$$

where $P^{\mathrm{neq}}_{\alpha\beta}$ is the nonequilibrium pressure tensor in the form required for the Navier-Stokes equation,

$$P^{\mathrm{neq}}_{\alpha\beta} = -\tau\rho T\left[\partial_\alpha\left(\frac{j_\beta}{\rho}\right) + \partial_\beta\left(\frac{j_\alpha}{\rho}\right) - \delta_{\alpha\beta}\partial_\gamma\left(\frac{j_\gamma}{\rho}\right)\right], \tag{18}$$

while $P''_{\alpha\beta}$ is the deviation of the nonequilibrium pressure tensor from $P^{\mathrm{neq}}_{\alpha\beta}$:

$$\partial_\gamma P''_{x\gamma} = -\frac{\tau}{2}\partial_x\left[\partial_x\left(j_x(1-3T) - \frac{j_x^3}{\rho}\right) - \partial_y\left(j_y(1-3T) - \frac{j_y^3}{\rho}\right)\right],$$

$$\partial_\gamma P''_{y\gamma} = -\frac{\tau}{2}\partial_y\left[\partial_y\left(j_y(1-3T) - \frac{j_y^3}{\rho}\right) - \partial_x\left(j_x(1-3T) - \frac{j_x^3}{\rho}\right)\right]. \tag{19}$$

In order to recover the Navier-Stokes equation, we will need to introduce additional terms into Eq. (16) in order to annihilate the right-hand side of the momentum equation (17) (See Sec. IV).

C. Deviations in the energy equation

Similarly, the energy density equation reads

$$\partial_t\left(\frac{j^2}{\rho} + 2\rho T\right) + \partial_\alpha q^{\mathrm{MB}}_\alpha + \partial_\alpha q^{\mathrm{neq}}_\alpha = -\partial_\alpha q'_\alpha - \partial_\alpha q''_\alpha, \tag{20}$$

where

$$q^{\mathrm{neq}}_\alpha = -4\tau\rho T\partial_\alpha T + 2\left(\frac{j_\beta}{\rho}\right)P^{\mathrm{neq}}_{\alpha\beta} \tag{21}$$

is the nonequilibrium energy flux required in the Fourier equation for the energy density. The first term in Eq. (21) is the Fourier law of energy dissipation, whereas the second term represents viscous dissipation. Again, terms in the right-hand side of Eq. (20) express the deviation of the energy equation from the required form. The first of these terms is given by Eqs. (15) and (13), while the result for the second term, q''_α, is given by the following expression:

$$\begin{aligned} q''_\alpha = {} & 3\tau\rho T\partial_\alpha T - \tau\left[\frac{3j_\alpha j_\alpha}{\rho^2}\partial_\alpha(\rho T) + 3j_\alpha T\partial_\beta\left(\frac{j_\beta}{\rho}\right) - \frac{3j_\alpha j_\beta}{2\rho}\partial_\beta T\right] \\ & - \tau\left\{(1-3T)\left[\partial_\beta\left(\frac{j_\alpha j_\beta}{\rho}\right) - \frac{j_\alpha}{2\rho}\partial_\beta j_\beta\right]\right\} \\ & - \tau\left[2\frac{j_\alpha^3}{\rho^3}\partial_\beta j_\beta + \frac{3j_\alpha j_\alpha}{\rho^2}\partial_\beta\left(\frac{j_\alpha j_\beta}{\rho}\right) + \frac{j_\alpha}{2\rho}\partial_\beta\left(\frac{j_\beta^3}{\rho^2}\right)\right] + \tau\partial_\beta e''_{\alpha\beta}, \end{aligned} \tag{22}$$

where

$$e''_{xx} = \frac{j_x j_x}{\rho} + \frac{j_x^4}{\rho^3},$$

$$e''_{yy} = \frac{j_y j_y}{\rho} + \frac{j_y^4}{\rho^3}, \tag{23}$$

$$e''_{xy} = \frac{j_x j_y j^2}{\rho^3}.$$

It should be noted that, in certain situations, many terms in Eqs. (22) and (23) can be safely neglected. For example, deviations of the order j^4 affect the viscous heat dissipation and can be ignored in cases where viscous heating is unimportant. However, we shall use the full expressions (22) and (23) for the deviation in the numerical implementation below.

The deviations in the hydrodynamic equations identified in this section are due to the lattice constraints of the $D2Q9$ lattice, and they cannot be removed by introducing a set of equilibrium distribution functions different from Eq. (8). These deviations can be removed only by introducing correction terms into the kinetic equation which we address in the next section.

IV. CORRECTION OF BGK EQUATION

To this end, we have computed the deviations due to the lattice constraints. In this section, an efficient way to remove these deviations by adding correction terms in the Boltzmann equation is introduced:

$$\partial_t f_i + c_{i\alpha}\partial_\alpha f_i = -\frac{1}{\tau}(f_i - f_i^{\mathrm{eq}}) + \Psi_i + \Phi_i. \tag{24}$$

The purpose of the Ψ_i terms is to correct the momentum equation, while the purpose of the Φ_i terms is to correct the energy equation.

A. Momentum equation correction terms Ψ_i

We require that the Ψ_i term affects only the momentum equation and delivers there a term which compensates $-\partial_\gamma P''_{\alpha\gamma}$. Thus

$$\sum_{i=0}^{8}\Psi_i = 0,$$

$$\sum_{i=0}^{8} c_{i\alpha}\Psi_i = \partial_\gamma P''_{\alpha\gamma},$$

$$\sum_{i=0}^{8} c_i^2\Psi_i = 0,$$

$$\sum_{i=0}^{8} c_{i\alpha}c_{i\beta}\Psi_i = 0,$$

$$\sum_{i=0}^{8} c_{i\alpha} c_i^2 \Psi_i = 0,$$

$$\sum_{i=0}^{8} c_{i\alpha} c_{i\beta} c_i^2 \Psi_i = 0. \quad (25)$$

Among these equations only nine are independent, and the unique solution is

$$\Psi_0 = 0,$$

$$\Psi_1 = \partial_\gamma P''_{x\gamma},$$

$$\Psi_2 = \partial_\gamma P''_{y\gamma},$$

$$\Psi_3 = -\partial_\gamma P''_{x\gamma},$$

$$\Psi_4 = -\partial_\gamma P''_{y\gamma}, \quad (26)$$

$$\Psi_5 = -\frac{1}{4}(\partial_\gamma P''_{x\gamma} + \partial_\gamma P''_{y\gamma}),$$

$$\Psi_6 = \frac{1}{4}(\partial_\gamma P''_{x\gamma} - \partial_\gamma P''_{y\gamma}),$$

$$\Psi_7 = \frac{1}{4}(\partial_\gamma P''_{x\gamma} + \partial_\gamma P''_{y\gamma}),$$

$$\Psi_8 = \frac{1}{4}(-\partial_\gamma P''_{x\gamma} + \partial_\gamma P''_{y\gamma}).$$

B. Energy equation correction terms Φ_i

Similarly, it is required that Φ_i terms appear only in the energy equation,

$$\sum_{i=0}^{8} \Phi_i = 0,$$

$$\sum_{i=0}^{8} c_{i\alpha} \Phi_i = 0,$$

$$\sum_{i=0}^{8} c_i^2 \Phi_i = \partial_\alpha (q'_\alpha + q''_\alpha),$$

$$\sum_{i=0}^{8} c_{ix} c_{iy} \Phi_i = 0,$$

$$\sum_{i=0}^{8} c_{i\alpha} c_i^2 \Phi_i = 0,$$

$$\sum_{i=0}^{8} c_{i\alpha} c_{i\beta} c_i^2 \Phi_i = 0. \quad (27)$$

The solution of that system is

$$\Phi_0 = -\frac{3}{2}\partial_\alpha (q'_\alpha + q''_\alpha),$$

$$\Phi_1 = \frac{1}{2}\partial_\alpha (q'_\alpha + q''_\alpha),$$

$$\Phi_2 = \frac{1}{2}\partial_\alpha (q'_\alpha + q''_\alpha),$$

$$\Phi_3 = \frac{1}{2}\partial_\alpha (q'_\alpha + q''_\alpha),$$

$$\Phi_4 = \frac{1}{2}\partial_\alpha (q'_\alpha + q''_\alpha), \quad (28)$$

$$\Phi_5 = -\frac{1}{8}\partial_\alpha (q'_\alpha + q''_\alpha),$$

$$\Phi_6 = -\frac{1}{8}\partial_\alpha (q'_\alpha + q''_\alpha),$$

$$\Phi_7 = -\frac{1}{8}\partial_\alpha (q'_\alpha + q''_\alpha),$$

$$\Phi_8 = -\frac{1}{8}\partial_\alpha (q'_\alpha + q''_\alpha).$$

C. Variable Prandtl number

A thermal lattice Boltzmann model should be able to simulate fluids with an arbitrary Prandtl number. The Prandtl number Pr is defined as the ratio of the viscosity and the thermal conductivity,

$$\mathrm{Pr} = \frac{c_p \mu}{\kappa}, \quad (29)$$

where c_p is specific heat under a constant pressure. We here suggest the following simple way to change the Prandtl number in the present model by adjusting the correction term Φ_i. In order to do this, we first note that, with the use of the guided equilibrium populations, the BGK model (16) leads to Pr=4, the same as the original consistent LB method [9]. Applying the correction for the energy equation mentioned in the previous section, the Prandtl number becomes Pr=1, as in the standard continuous BGK model. This happens because the correction compensates, among the others, the term,

$$3\tau\rho T \partial_\alpha T$$

[first term in Eq. (22)], responsible for the change of the thermal conductivity of the model. Thus arbitrary values of

Pr can be obtained by applying the following transformation in Eq. (22) and thereby altering the counterterm Φ_i in the term

$$3\tau\rho T\partial_\alpha T \to \frac{(4-\mathrm{Pr})}{\mathrm{Pr}}\tau\rho T\partial_\alpha T. \tag{30}$$

Thus with the simple transform (30) in the energy correction term Φ_i, kinetic equation (24) recovers the hydrodynamic equations with a predetermined Prandtl number. In Sec. VI, we shall validate this in the thermal Couette flow for fluids with various Prandtl numbers.

D. Gravity force

Flows subject to external forces, such as gravity, are a major concern in many applications. In order to incorporate the force ρg, where g is the acceleration due to gravity, it suffices to apply the following transformation when calculating the correction terms Ψ_i:

$$\partial_\beta P''_{\alpha\beta} \to \partial_\beta P''_{\alpha\beta} + \rho g_\alpha. \tag{31}$$

Any additional physics can be incorporated into the present model by similar considerations.

E. Corrected hydrodynamic equations

Taking into account all the aforementioned correction terms Ψ_i and Φ_i in the kinetic equation (24), and using again the Chapman-Enskog analysis, we obtain the two-dimensional Navier-Stokes and Fourier hydrodynamic equations for density, momentum, and temperature:

$$\partial_t \rho = -\partial_\gamma(\rho u_\gamma),$$

$$\partial_t u_\alpha = -u_\gamma\partial_\gamma u_\alpha - \frac{1}{\rho}\partial_\alpha(\rho T) + \frac{1}{\rho}\partial_\gamma[\tau\rho T(\partial_\alpha u_\gamma + \partial_\gamma u_\alpha - \partial_\kappa u_\kappa \delta_{\alpha\gamma})] + \rho g_\alpha, \tag{32}$$

$$\partial_t T = -u_\alpha\partial_\alpha T - T\partial_\alpha u_\alpha - \frac{1}{\rho}\left[\partial_\alpha\left(\frac{2}{\mathrm{Pr}}\tau\rho T\partial_\alpha T\right) + (\partial_\gamma u_\alpha)\tau\rho T(\partial_\alpha u_\gamma + \partial_\gamma u_\alpha - \partial_\kappa u_\kappa\delta_{\alpha\gamma})\right].$$

The fluid corresponds to the ideal gas equation of state, $p=\rho T$, with specific heats $c_v=1.0$ and $c_p=2.0$, in lattice units, and with the adiabatic exponent $\gamma=c_p/c_v=2.0$. The viscosity coefficient μ and thermal conductivity κ can be identified as

$$\mu = \tau\rho T, \quad \kappa = \frac{2}{\mathrm{Pr}}\tau\rho T. \tag{33}$$

The Prandtl number is a tunable parameter and can take arbitrary values. A wide range of gases and fluids whose physics is described by Eq. (32) can be simulated. We now proceed with a time-space discretization of the kinetic equation (24).

V. LATTICE BOLTZMANN DISCRETIZATION

Derivation of the lattice Boltzmann scheme for the kinetic equation (24) proceeds essentially along the lines of Ref. [6]. First, we integrate over the time step δt along the characteristics:

$$f_i(x+c_i\delta t, t+\delta t) = f_i(x,t) + \int_t^{t+\delta t}\frac{1}{\tau}[f_i^{\mathrm{eq}}(t') - f_i(t')]dt' + \int_t^{t+\delta t}\Psi_i(t')dt' + \int_t^{t+\delta t}\Phi_i(t')dt'. \tag{34}$$

The time integrals of the collision term as well as of the correction terms is evaluated using the second-order accurate trapezoidal rule. Second, in order to establish a semi-implicit scheme, the following transformation is applied [6]:

$$g_i = f_i + \frac{\delta t}{2\tau}(f_i - f_i^{\mathrm{eq}}) - \frac{\delta t}{2}[\Psi_i + \Phi_i]. \tag{35}$$

This leads to a semiexplicit scheme,

$$g_{t+\delta t} = g_t + \frac{2\delta t}{\delta t + 2\tau}[f_t^{\mathrm{eq}} - g_t] + \frac{2\tau\delta t}{\delta t + 2\tau}[\Psi_t(f) + \Phi_t(f)]. \tag{36}$$

Note that the simple scheme (36) is semiexplicit due to the presence of the correction terms Ψ_i and Φ_i (and not fully explicit, as in the standard case without any corrections). The scheme utilizes the transformed populations g. The equilibrium f^{eq} can be computed using equations that relate the locally conserved moments of the populations f with those of the g populations. In order to do this, we evaluate the moments of the transformation (35):

$$\rho(f) = \rho(g), \tag{37}$$

$$j_x(f) = j_x(g) + \frac{\delta t}{2}\sum_{i=0}^{8} c_{ix}\Psi_i(f), \tag{38}$$

$$j_y(f) = j_y(g) + \frac{\delta t}{2}\sum_{i=0}^{8} c_{iy}\Psi_i(f), \tag{39}$$

$$T(f) = \frac{1}{2\rho}\left(\sum_{i=0}^{8} c_i^2 g_i - \frac{j^2(f)}{\rho} + \frac{\delta t}{2}\sum_{i=0}^{8} c_i^2\Phi_i(f)\right). \tag{40}$$

The above set of equations can be simplified using Eqs. (26) and (28):

$$\rho(f) = \rho(g), \tag{41}$$

$$j_x(f) = j_x(g) + \frac{\delta t}{2}[\partial_\gamma P''_{x\gamma}(f)], \tag{42}$$

$$j_y(f) = j_y(g) + \frac{\delta t}{2}[\partial_\gamma P''_{y\gamma}(f)], \tag{43}$$

$$T(f) = \frac{1}{2\rho}\left(\sum_{i=0}^{8} c_i^2 g_i - \frac{j^2(f)}{\rho} + \frac{\delta t}{2}\partial_\alpha[q'_\alpha(f) + q''_\alpha(f)]\right). \tag{44}$$

Finally, discretization in space is done as in the standard lattice Boltzmann method: if x is a grid node then also $x \pm c_i \delta t$ is the grid node.

In the simulation, the following algorithm was implemented for the collision step.

Step 1. Calculate ρ, j_α, and T using Eqs. (41)–(44), $(\partial_\gamma P''_{\alpha\gamma})^{t-1}$, $[\partial_\alpha(q'_\alpha + q''_\alpha)]^{t-1}$, and g_t values.

Step 2. Calculate $(\partial_\gamma P''_{\alpha\gamma})^t$ and $[\partial_\alpha(q'_\alpha + q''_\alpha)]^t$ using values of ρ, j_α, and T from Step 1.

Step 3. Calculate again ρ, j_α, and T using Eqs. (41)–(44), g_t, and the values calculated in Step 2.

Step 4. Use ρ, j_α, and T from Step 3 for the calculation of the equilibrium values (8).

Step 5. Use $(\partial_\gamma P''_{\alpha\gamma})^t$ and $[\partial_\alpha(q'_\alpha + q''_\alpha)]^t$ from Step 2 in the discrete equation (36) along with the equilibrium values calculated in Step 4.

The terms $\partial_\gamma P''_{\alpha\gamma}$ and $\partial_\alpha(q'_\alpha + q''_\alpha)$ are evaluated using a second-order accurate finite-difference scheme.

A few comments on the computational efficiency of our model are in order. First, the present thermal model is only about 2.7 times slower as compared to the standard isothermal LB method on the same $D2Q9$ lattice due to evaluations of the deviation terms (19) and (22). Note that, depending on the desired accuracy and the optimization level, faster and simpler algorithms can be readily designed. For example, for the natural convection problem considered below in Sec. VI, deviations of the order j^3, $j^2\Delta T$, and j^4 can be safely neglected in the energy equation, which removes the computational overhead with respect to the standard isothermal $D2Q9$ code without sacrificing the accuracy of the results in the thermal case. It should be stressed that optimization of the code was not pursued in the present study so that the above estimates are only qualitative.

Second, as compared to the thermal model on two lattices [6] in terms of memory use, the present model requires storage of 12 values per node, that is, nine for the populations g_i, two for the terms $(\partial_\gamma P''_{\alpha\gamma})^t$, and one for the term $[\partial_\alpha(q'_\alpha + q''_\alpha)]^t$. In the case of the two distribution function thermal models [6], the storage of at least 18 values per node is required, without taking into account the additional computational effort needed in order to recover viscous dissipation terms.

These estimates show that the present one-lattice thermal model is viable. We shall now proceed with a numerical validation of the present scheme.

VI. NUMERICAL EXAMPLES

In this section, the thermal model developed above is validated numerically. Equilibrium populations are expanded until the fourth order in the velocity and the corrections described in previous sections are applied. The same model is used in all simulations, even though viscous heat dissipation could have been ignored in the Rayleigh-Bénard setup.

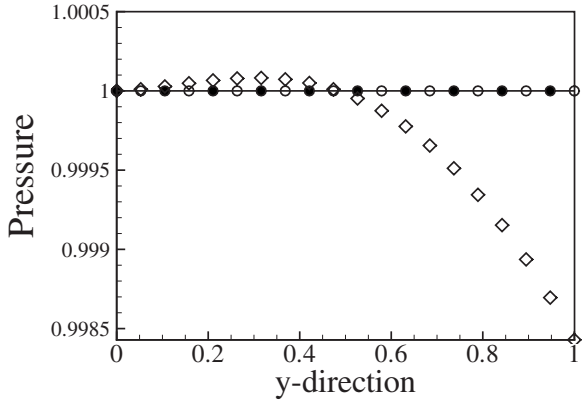

FIG. 2. Pressure $p=\rho T$ as a function of the reduced y coordinate ($y_{\text{norm}}=y/H$, H is the distance between the plates) in the thermal Couette flow. Line: analytical solution (46); open circles: LB model with guided equilibrium; filled circles: LB model with guided equilibrium and correction terms; and diamonds: LB model [7,9]. Reynolds number Re=320.

A. Necessity of guided equilibrium

In our first example, we compare the three different models: the original consistent LB model [7,9], the model using the guided equilibrium (8) without any correction terms, and the full model after the correction terms are applied. In order to demonstrate the necessity of the guided equilibrium, we simulate the two-dimensional Couette flow between two parallel moving plates at different temperatures. Isothermal walls are separated by a distance H and move parallel to the x axis. The diffusive wall boundary conditions [12] are implemented for the isothermal walls, and a periodic boundary condition is applied for the rest. Analysis similar to the one presented in [13] results in the following relation at the steady state:

$$P - N^{\text{eq}} = \text{const}, \tag{45}$$

where $P \equiv P^{\text{eq}} = P_{xx} + P_{yy}$ is the trace of the pressure tensor and $N = P_{xx} - P_{yy}$ is the normal stress difference. On one hand, using the guided equilibrium (8) in Eq. (45) results in the constant pressure in the whole domain:

$$\rho T = \text{const}. \tag{46}$$

This is consistent with the correct Maxwell-Boltzmann relation for the pressure tensor. On the other hand, as we have already mentioned in Sec. II, the equilibrium normal stress difference N^{eq} of the consistent LB model [7,9] exhibits a deviation of the order $\sim j^2\Delta T$, where ΔT is a variation around the reference temperature $T_0 = 1/3$. In this case, Eq. (45) yields a different result, namely, the pressure $p=\rho T$ varies along the y axis according to the variation of the momentum,

$$\rho T - \frac{(1-3T)}{4T}\frac{j_x^2}{\rho} = \text{const}. \tag{47}$$

In Fig. 2, simulation results for the pressure in the Couette flow with all three models are presented and compared with the analytical solution (46). While the variation of the pres-

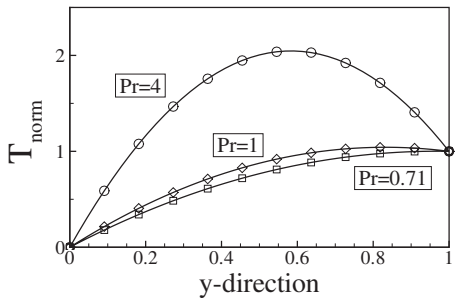

FIG. 3. Temperature profile in the thermal Couette flow. Plotted is the reduced temperature, $T_{\text{norm}}=(T-T_{\text{cold}})/(T_{\text{hot}}-T_{\text{cold}})$, versus the reduced y coordinate (as in Fig. 2). Eckert number Ec=3. Line: analytical solution for Pr=4, 1, and 0.71. Reynolds number Re =200. Symbol: Simulation results for the three cases (see text). Diamonds: Case 1; squares: Case 2 (air); and circles: Case 3.

sure $p=\rho T$ away from the constant value is numerically small for the original model [7,9], it is still visible, and it verifies the analytical solution (47) rather than Eq. (46). On the other hand, the LB model with the guided equilibrium verifies the constancy of the pressure with machine precision. The same holds also for the LB model with the guided equilibrium when all the correction terms are applied, as expected. This demonstrates the necessity of the guided equilibrium in our construction.

B. Viscous heat dissipation

We simulate the thermal Couette flow as in the preceding section but for small temperature differences. In this case, the viscous heat dissipation is important and affects the temperature profile. As is well-known, the Navier-Stokes and Fourier equations (32) predict that the temperature profile depends on the Prandtl number, Pr, and on the Eckert number, Ec, where

$$\text{Ec}=\frac{u^2}{c_p\Delta T}, \tag{48}$$

with u the difference of the velocities of the plates, and ΔT the difference of temperatures of the plates. This simulation enables one to verify that the correction terms do recover the right Prandtl number. In the simulation, we used Ec=3 and $\Delta T=2\times 10^{-4}T_0$, where $T_0=1/3$ is the reference temperature. Three different cases were considered.

Case 1. LB with the guided equilibrium (8) and the corrections Ψ_i and Φ_i which deliver Pr=1 (that is, without the transformation (30).

Case 2. As in Case 1 plus the transformation (30) to match Pr=0.71 (air).

Case 3. As in Case 1 plus the transformation (30) to match Pr=4.

Simulation results for the temperature profile are presented in Fig. 3, and are in excellent agreement with the analytical solution. For the current setup, with the present implementation of the boundary condition, simulation results remain in agreement with the analytical solution for Prandtl numbers ranging from 0.01 to 20.

C. Rayleigh-Bénard convection

The Rayleigh-Bénard convection flow is a classical benchmark on the thermal models. The fluid is enclosed between two parallel stationary walls, the hot (bottom) and the cold (top), and experiences the gravity force. Density variations caused by the temperature variations drive the flow, while the viscosity will counteract to equilibrate it.

In our LB model, gravity is implemented using the correction (31). We operate the model in the weakly compressible regime, however, without using the Boussinesq approximation. For that we set a temperature difference of the order of 3% of the reference temperature $T_0=1/3$. At the top and the bottom walls we apply the diffusive wall boundary condition [12], whereas the periodic boundary condition is applied on the vertical walls. For the nodes that belong to the isothermal walls, gravitational force was not applied.

The Prandtl number used corresponds to air, Pr=0.71. The dimensionless number that characterizes the flow is the Rayleigh number Ra,

$$\text{Ra}=\frac{\text{Pr}\,g\beta\Delta T H^3}{\nu^2}, \tag{49}$$

where g is the gravity acceleration, ΔT is the wall temperature difference, H is the distance between the walls, and ν is the kinematic viscosity of the fluid. For the ideal gas equation of state, the thermal expansion coefficient β is defined as

$$\beta=-\frac{1}{\rho}\left(\frac{\partial\rho}{\partial T}\right)_P=\frac{1}{T}. \tag{50}$$

For the computation of the Rayleigh number, we used the thermal expansion coefficient evaluated at the reference temperature $T_0=1/3$, that is, $\beta=3$. The heat transfer is described by the Nusselt number, Nu, defined as the ratio between convective heat transport to the heat transport due to temperature conduction:

$$\text{Nu}=1+\frac{\langle u_y T\rangle H}{\kappa\Delta T}. \tag{51}$$

Here $\langle u_y T\rangle$ denotes the average over the convection layer and κ is the thermal conductivity of the model (33). For the current simulations, a computation domain with the aspect ratio 2:1 was considered.

For this setup, the critical Rayleigh number was found to be $\text{Ra}_{\text{cr}}=1700\pm 10$, which is consistent with the reference data for the Boussinesq approximation [14,15]. Any flow field was dissipated for values less than Ra_{cr}. On the contrary, for values larger than Ra_{cr}, the flow develops two or more cells (vortices) depending on the initial conditions.

For different Rayleigh numbers, simulations for the 51, 101, and 201 grid nodes in the y direction were performed. Extrapolating the obtained values of the Nusselt number, an estimate of the final converged solution can be done (Nu_{R}). In Fig. 4, the isotherms of $\text{Ra}=10^4$ and 5×10^4 are plotted for the case of 101 grid nodes in the y direction. In Fig. 5, the contours of the stream function of the compressible flow field for $\text{Ra}=10^4$ and 5×10^4 are plotted. The extrapolated converged values of the Nusselt number at various Rayleigh numbers are plotted in Fig. 6 and compared with the standard

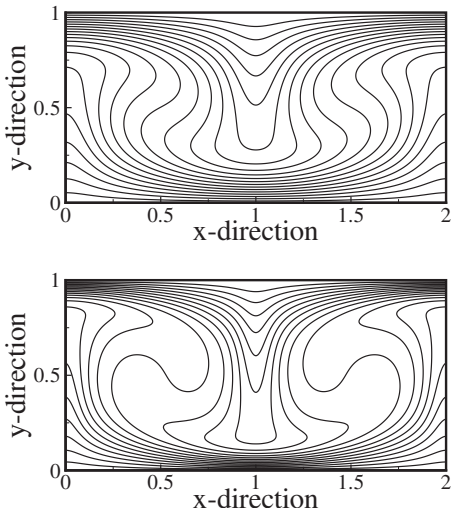

FIG. 4. Contour plot with 19 equidistant isotemperature lines for $\mathrm{Ra}=10^4$ (top) and $\mathrm{Ra}=5\times10^4$ (bottom).

reference data [14,15] in Table I. The present model is found to be in good agreement with [14], and it also agrees well with the thermal LB models on double lattices where the temperature dynamics is treated as a passive scalar [6,16]. It should be noted that for Ra up to 10^4 a uniform grid with 51 nodes in the y direction was sufficient, while for larger values of Ra, larger grids provide more accurate results. In Fig. 7, a grid convergence study is performed. Natural convection of $\mathrm{Ra}=3\times10^4$ in the same setup is considered. Figure 7 reveals the second-order accuracy of the numerical scheme.

Finally, it should be mentioned that on a grid with only 51 nodes in the y direction, the code was run stably for Ra as high as at least 10^8 which proves a good numerical stability of the algorithm. In Fig. 8, a snapshot of the temperature field is presented at $\mathrm{Ra}=10^8$. However, a study of the natural convection at high Rayleigh numbers is out of the scope of this paper.

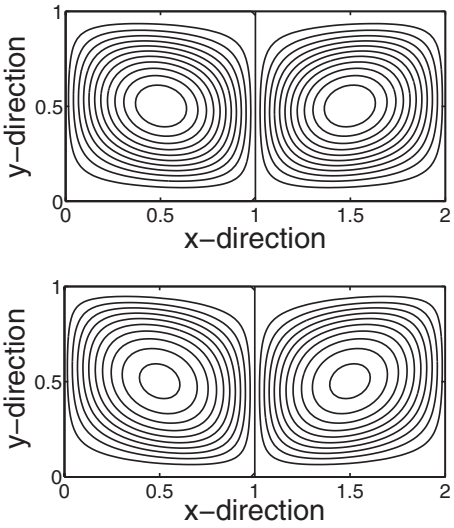

FIG. 5. Stream function contours for $\mathrm{Ra}=10^4$ (top) and $\mathrm{Ra}=5\times10^4$ (bottom). The difference between contour lines is 0.025 in units of $\rho_{max}U_{max}H$.

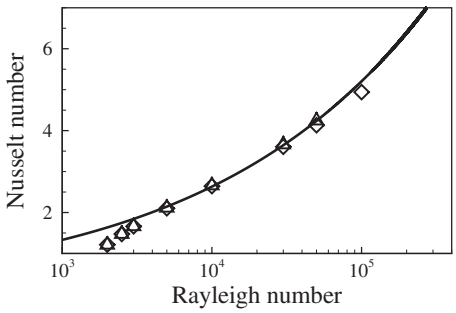

FIG. 6. Rayleigh Bénard convective flow. Nusselt number vs Rayleigh number. Diamonds: the current LB model; triangles: reference data of Ref. [14]; and line: Empirical power-law $\mathrm{Nu}=1.56(\mathrm{Ra}/\mathrm{Ra}_c)^{0.296}$ [14].

VII. SUMMARY

A reader who wishes to implement this model should execute the following steps.

(1) Use guided equilibrium populations (8).

(2) Calculate the correction terms Ψ_i and Φ_i with a second-order finite-difference scheme.

(3) Use the discretized equation (36).

VIII. CONCLUSION

In this paper, we have developed a lattice Boltzmann model for simulation of thermal flows with the standard and most commonly used $D2Q9$ lattice. The important starting point of the derivation is the consistent LB method [7]. Unlike the previous approaches, the consistent LB model on standard lattices already includes energy as a locally conserved quantity, the nonequilibrium stress tensor is free of a spurious bulk viscosity, and a part of the moment relations satisfies the required Maxwell-Boltzmann relations. Hence, by using the consistent LB model, it becomes unnecessary to introduce a separate lattice for the energy field.

We have considerably refined the consistent LB model in two steps. First, following the concept of guided equilibrium [8], we recovered Galilean invariance of the pressure tensor at nonvanishing variations of the temperature. Second, we have identified the remaining deviations in the Navier-Stokes-Fourier equations and have removed them by adding compensating terms into the kinetic equation. This step also

TABLE I. Simulation results of the present model compared to the simulation results of Ref. [14]. Left column: Rayleigh number; central column: Nusselt number; and right column: difference in percent from the values of Ref. [14].

Rayleigh number	Nusselt number ($\mathrm{Nu_R}$)	Difference from Ref. [14] (%)
2500	1.474	0.07
5000	2.104	0.57
10000	2.644	0.64
30000	3.605	1.56
50000	4.133	2.64

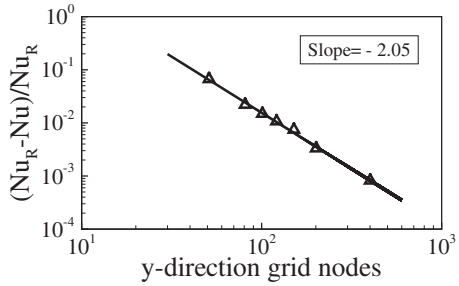

FIG. 7. Grid convergence study for $\mathrm{Ra}=3\times10^4$. Symbol: The relative error between the simulation result Nu and the converged solution $\mathrm{Nu_R}$. The line is a fitted curve that reveals second-order convergence.

allowed us to make the Prandtl number a tunable parameter, and to add external forces. It should be noted that additional terms also appear in the method based on two lattices [6] but there is no relation between both. On the other hand, a numerical implementation of the kinetic equation with additional terms here is practically not much different from the method first developed in [6]. Finally, it is straightforward to extend the present model to three dimensions based on the $D3Q27$ consistent LB model [7].

We shall conclude this paper with a general comment on the construction of thermal lattice Boltzmann models. As we already mentioned in the Introduction, there are two basic directions for such a development, one which uses larger and more isotropic sets of velocities, and the other which uses a small number of velocities and introduces nonlocal (dependent on the gradients of the fields) corrections to compensate for the deficit of lattice symmetry. This situation resembles the classical dilemma of extending the hydrodynamics beyond the Navier-Stokes level: One way is the higher-order hydrodynamics (Burnett or super-Burnett) which means higher-order derivatives and more nonlocality in the equations for the standard hydrodynamic fields. The other is to take more moments while staying local (Grad's moment method). Both approaches have positive and negative aspects. In our case, the attractive features of large velocity sets (locality, isotropy, possibility of the exact treatment of propagation) should be waged against the necessity of handling many more fields (populations). On the other hand, the obvious attractive side of the small lattices approach has to be opposed by the fact that one has to evaluate more terms dependent on the gradients of the fields. While this proves to be possible, still, one needs to be careful about numerical

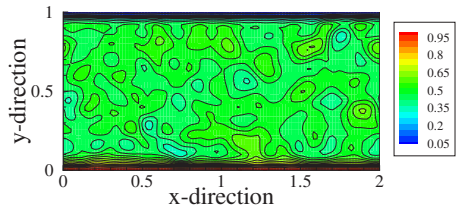

FIG. 8. (Color online) Snapshot of the temperature field at $\mathrm{Ra}=10^8$, $\mathrm{Pr}=0.71$, using a uniform grid of 51 nodes for the y direction. Contours of reduced temperature, $T_{\mathrm{norm}}=(T-T_{\mathrm{cold}})/(T_{\mathrm{hot}}-T_{\mathrm{cold}})$ are plotted.

errors brought in by such procedures. We believe that both these approaches, at present, show advantages and disadvantages, so the decision about which to prefer should be the focus of future studies.

ACKNOWLEDGMENTS

We are indebted to our colleagues S. Ansumali, S. Arcidiacono, K. Boulouchos, S. Chikatamarla, C. Frouzakis, and J. Mantzaras for their help, questions, and discussions. We gratefully acknowledge support by BFE Project No. 100862, CCEM-CH, and by ETH Project No. 0-20235-05.

APPENDIX: DERIVATION OF HYDRODYNAMIC EQUATIONS

We apply the Chapman-Enskog expansion in order to derive hydrodynamic equations corresponding to the BGK equation (16) with the equilibrium (8). Populations f_i and the time derivative operator are expanded into powers of the relaxation parameter τ,

$$f_i = f_i^{eq} + \sum_{n=1}^{\infty} f_i^{(n)} \tau^n, \tag{A1}$$

$$\partial_t = \sum_{n=0}^{\infty} \tau^n \partial_t^{(n)}. \tag{A2}$$

The nonequilibrium pressure tensor and energy flux to first order in τ are defined as

$$P_{\alpha\beta}^{(1)} = \tau \sum_{i=0}^{8} c_{i\alpha} c_{i\beta} f_i^{(1)}, \quad q_\alpha^{(1)} = \tau \sum_{i=0}^{8} c_{i\alpha} c_i^2 f_i^{(1)}. \tag{A3}$$

On the zeroth order, equations for density, momentum, pressure tensor, and energy flux are

$$\partial_t^{(0)} \rho = -\partial_\alpha j_\alpha, \tag{A4}$$

$$\partial_t^{(0)} j_\alpha = -\partial_\beta P_{\alpha\beta}^{\mathrm{MB}}, \tag{A5}$$

$$\partial_t^{(0)} \left[\frac{j^2}{\rho} + 2\rho T \right] = -\partial_\alpha q_\alpha^{\mathrm{MB}} - \partial_\alpha q'_\alpha, \tag{A6}$$

$$\partial_t^{(0)} P_{\alpha\beta}^{\mathrm{eq}} = -\partial_\gamma Q_{\alpha\beta\gamma}^{\mathrm{eq}} - \frac{1}{\tau} P_{\alpha\beta}^{(1)}, \tag{A7}$$

$$\partial_t^{(0)} q_\alpha^{\mathrm{eq}} = -\partial_\beta R_{\alpha\beta}^{\mathrm{eq}} - \frac{1}{\tau} q_\alpha^{(1)}, \tag{A8}$$

where $Q_{\alpha\beta\gamma}^{\mathrm{eq}}$ and $R_{\alpha\beta}^{\mathrm{eq}}$ are the third- and the fourth-order moments evaluated at the local equilibrium (8) (the explicit form of these function was given in Sec. II). From Eq. (A6), we derive the zeroth-order equation for the temperature

$$\partial_t^{(0)} T = -T\partial_\alpha \left(\frac{j_\alpha}{\rho} \right) - \frac{j_\alpha}{\rho} \partial_\alpha T - \frac{1}{2\rho} \partial_\alpha q'_\alpha. \tag{A9}$$

On the first order in τ we need equations for the locally conserved fields only,

$$\partial_t^{(1)}\rho = 0, \tag{A10}$$

$$\partial_t^{(1)} j_\alpha = -\frac{1}{\tau}\partial_\beta P_{\alpha\beta}^{(1)}, \tag{A11}$$

$$\partial_t^{(1)}\left[\frac{j^2}{\rho} + 2\rho T\right] = -\frac{1}{\tau}\partial_\alpha q_\alpha^{(1)}. \tag{A12}$$

Function $P_{\alpha\beta}^{(1)}$ is represented as a sum of two terms, $P_{\alpha\beta}^{\mathrm{neq}}$, which results in the correct Navier-Stokes term in the momentum equation, and $P''_{\alpha\beta}$, representing the deviation:

$$P_{\alpha\beta}^{(1)} = P_{\alpha\beta}^{\mathrm{neq}} + P''_{\alpha\beta}, \tag{A13}$$

$$P_{\alpha\beta}^{(1)} = -\tau[\partial_\gamma Q_{\alpha\beta\gamma}^{\mathrm{eq}} + \partial_t^{(0)} P_{\alpha\beta}^{\mathrm{eq}}], \tag{A14}$$

$$P_{\alpha\beta}^{\mathrm{neq}} = -\tau[\partial_\gamma Q_{\alpha\beta\gamma}^{\mathrm{MB}} + \partial_t^{(0)} P_{\alpha\beta}^{\mathrm{MB}}]. \tag{A15}$$

In order to derive $P_{\alpha\beta}^{(1)}$ from Eq. (A7), we note that the left-hand side can be computed by the chain rule,

$$\partial_t^{(0)} P_{\alpha\beta}^{\mathrm{eq}} = \frac{\partial P_{\alpha\beta}^{\mathrm{eq}}}{\partial\rho}\partial_t^{(0)}\rho + \frac{\partial P_{\alpha\beta}^{eq}}{\partial j_\gamma}\partial_t^{(0)} j_\gamma + \frac{\partial P_{\alpha\beta}^{\mathrm{eq}}}{\partial T}\partial_t^{(0)} T. \tag{A16}$$

Using Eqs. (A4)–(A6) and (A16) in Eq. (A7), we obtain

$$P_{\alpha\beta}^{\mathrm{neq}} = -\tau\rho T\left[\partial_\alpha\left(\frac{j_\beta}{\rho}\right) + \partial_\beta\left(\frac{j_\alpha}{\rho}\right) - \partial_\gamma\left(\frac{j_\gamma}{\rho}\right)\delta_{\alpha\beta}\right], \tag{A17}$$

$$P''_{\alpha\beta} = \tau\left(\frac{1}{2\rho}\right)\frac{\partial P_{\alpha\beta}^{\mathrm{eq}}}{\partial T}\partial_\gamma q'_\gamma - \tau\partial_\gamma Q'_{\alpha\beta\gamma}. \tag{A18}$$

Substituting Eqs. (A17) and (A18) into Eq. (A11), and combining the latter with Eq. (A5), and also combining Eq. (A4) with Eq. (A10), we derive the equations for the density and velocity $u_\alpha = j_\alpha/\rho$ to first order,

$$\partial_t\rho = -\partial_\alpha(\rho u_\alpha), \tag{A19}$$

$$\partial_t u_\alpha = -u_\beta\partial_\beta u_\alpha - \frac{1}{\rho}\partial_\alpha(\rho T) - \frac{1}{\rho}\partial_\beta\Pi_{\alpha\beta} - \frac{1}{\rho}\partial_\gamma P''_{\alpha\gamma}, \tag{A20}$$

where

$$\Pi_{\alpha\beta} = -\tau\rho T[\partial_\beta u_\alpha + \partial_\alpha u_\beta - (\partial_\gamma u_\gamma)\delta_{\alpha\beta}] \tag{A21}$$

is the nonequilibrium pressure tensor of a Newtonian fluid, and $P''_{\alpha\gamma}$ [Eq. (A18)] is the deviation. Expanding Eq. (A18), we arrive at the explicit form of the deviation, Eq. (A19).

Derivation of the equation for the energy (or, equivalently, for the temperature) is done in a similar way upon computing the first-order correction $q_\alpha^{(1)}$ from Eq. (A8). The resulting equation for the temperature reads

$$\partial_t T = -u_\alpha\partial_\alpha T - T\partial_\alpha u_\alpha - \frac{1}{\rho}[\partial_\alpha(2\tau\rho T\partial_\alpha T) - (\partial_\beta u_\alpha)\Pi_{\alpha\beta}] - \frac{1}{2\rho}\partial_\kappa q'_\kappa - \frac{1}{2\rho}\partial_\gamma q''_\gamma. \tag{A22}$$

The last two terms in this equation represent the deviation. Note that, unlike in the case of the momentum equation (A20), the deviation also includes a zero-order term q'_κ. This happens because, with the choice of the guided equilibrium (8), we have set the equilibrium pressure tensor in the required Maxwell-Boltzmann form but not the equilibrium energy flux (why the latter is impossible on the $D2Q9$ was explained in Sec. II). Finally, the first-order deviation [the last term in Eq. (A22)] has the form given by Eqs. (22) and (23).

[1] S. Succi, *The Lattice Boltzmann Equation for Fluid Dynamics and Beyond* (Oxford University Press, Oxford, 2001).
[2] H. Chen, S. Kandasamy, S. Orszag, R. Shock, S. Succi, and V. Yakhot, Science **301**, 633 (2003).
[3] S. Succi, I. V. Karlin, and H. Chen, Rev. Mod. Phys. **74**, 1203 (2002).
[4] S. Ansumali, I. V. Karlin, and H. C. Öttinger, Phys. Rev. Lett. **94**, 080602 (2005).
[5] S. S. Chikatamarla and I. V. Karlin, Phys. Rev. Lett. **97**, 190601 (2006).
[6] X. He, S. Chen, and G. D. Doolen, J. Comput. Phys. **146**, 282 (1998).
[7] S. Ansumali and I. V. Karlin, Phys. Rev. Lett. **95**, 260605 (2005).
[8] I. V. Karlin and S. Succi, Phys. Rev. E **58**, R4053 (1998).
[9] N. I. Prasianakis, S. S. Chikatamarla, I. V. Karlin, S. Ansumali, and K. B. Boulouchos, Math. Comput. Simul. **72**, 179 (2006).
[10] I. V. Karlin, A. Ferrante, and H. C. Öttinger, Europhys. Lett. **47**, 182 (1999).
[11] Y. H. Qian, D. d'Humieres, and P. Lallemand, Europhys. Lett. **17**, 479 (1992).
[12] S. Ansumali and I. V. Karlin, Phys. Rev. E **66**, 026311 (2002).
[13] S. Ansumali, I. V. Karlin, S. Arcidiacono, A. Abbas, and N. I. Prasianakis, Phys. Rev. Lett. **98**, 124502 (2007).
[14] R. M. Clever and F. H. Busse, J. Fluid Mech. **65**, 625 (1974).
[15] F. H. Busse, Rep. Prog. Phys. **41**, 1929 (1978).
[16] X. Shan, Phys. Rev. E **55**, 2780 (1997).